Article

Magnetohydrodynamics Williamson Nanofluid Flow over an Exponentially Stretching Surface with a Chemical Reaction and Thermal Radiation

Hillary Muzara [1] and Stanford Shateyi [2],*

[1] Department of Mathematics and Computational Sciences, University of Zimbabwe, Mt. Pleasant, Harare P.O. Box MP167, Zimbabwe; hmuzara@science.uz.ac.zw
[2] Department of Mathematical and Computational Sciences, University of Venda, P. Bag X5050, Thohoyandou 0950, South Africa
* Correspondence: stanford.shateyi@univen.ac.za

Abstract: Presented in this current study is the numerical analysis of magnetohydrodynamics Williamson nanofluid flow over an exponentially stretching surface. The most important aspect of the investigation is that the effects of the magnetic field, chemical reaction and thermal radiation in the fluid flow are taken into account. The partial differential equations governing the present Williamson nanofluid flow problem were observed to be highly nonlinear and coupled. Suitable similarity transformations were used to transmute the coupled system of nonlinear partial differential equations governing the fluid flow into a linear system. The linear system was solved numerically using the spectral quasi-linearization method. The MATLAB bvp4c numerical technique and a comparison with existing results for the skin friction coefficient were used to confirm the appropriateness of the method in solving the current problem. The influence of some pertinent physical parameters on the fluid's velocity, temperature and concentration profiles were displayed graphically. The effects of all the physical parameters on the skin friction coefficient, Nusselt number and Sherwood number were portrayed in a tabular form. It was noted that enhancing the thermal radiation parameter reduces the fluid's temperature, Nusselt number and the skin friction coefficient, while the Sherwood number is improved.

Keywords: magnetohydrodynamics; Williamson nanofluid; quasi-linearization; chemical reaction; thermal radiation

MSC: 65N12; 76M22; 76M25; 80M25

1. Introduction

Non-Newtonian fluids occur most often in industrial and engineering applications. The rheological properties of the non-Newtonian fluids cannot be explained using the famous Navier–Stokes equations. As a consequence, a number of models have been used to describe the characteristics of non-Newtonian fluids. These models include the Ellis model [1], Carreaus model [2], power law model [3], Cross model [4] and Casson model [5], to mention but a few. One special type of non-Newtonian model is the Williamson model [6], which was proposed to describe the flow of pseudoplastic materials. The boundary layer flow of the pseudoplastic materials has found applications in bio-engineering, chemical and nuclear industry, material processing and geophysics.

In fluid dynamics, Sakiadis [7] was the first researcher to study the boundary layer flow over a continuous stretching surface. An inaugural study of fluid flow of Blasius type past a stretching surface was initiated by Crane [8]. The study of fluid flow over a stretching sheet has been a subject of interest in recent years due to its significant importance in areas such as metallurgical processes, polymer extrusion, plastic films, metal spinning, etc. There

are quite a number of studies that have been performed on fluid flow past a stretching sheet, i.e., [9–13], among others.

In thermal engineering, the enhancement of the thermal characteristics of heat transfer fluids is a priority. The thermal conductivity and heat transfer qualities of the base fluid can be improved by dispersing nanosized (1–100 nm) solid particles into the fluid. These nanoparticles are usually metals, carbon nanotubes, oxides or carbines. The enhancement of heat transfer in fluids as a result of dispersing ultra-fine particles was first reported by Masuda et al. [14]. The term 'nanofluid', a fluid that contains dispersed nanoparticles, was introduced by Choi and Eastman [15]. A significant number of studies have been carried out on nanofluids, which inlcude the works by Elboughdiri et al. [16], Ashraf et al. [17], Nabwey et al. [18], Selimefendigil et al. [19] and Lou et al. [20].

Alfven [21] was the first to study the magnetic properties and the characteristics of fluids that are electrical conductors. Typical examples of such magnetofluids include electrolytes, plasmas, salt water and liquid metals. There has been growing interest in studying the MHD Williamson nanofluid. Abbas et al. [22] investigated the effects of heat generation and viscous dissipation on an MHD Williamson nanofluid that flows past a linear stretching sheet in a porous medium. The characteristics of MHD flow and heat transfer of a Williamson nanofluid flowing past a stretching sheet were examined by Reddy et al. [23]. Shawky et al. [24] used the Runge–Kutta method to analyze the heat and mass transfer of magnetohydrodynamic Williamson nanofluid flowing over a stretching sheet. The influence of Joule heating, heat generation/absorption, thermal radiation and chemical reaction on the MHD Williamson nanofluid flow over a stretching sheet through a porous medium was investigated by Bouslimi et al. [25]. Other notable works on the MHD Williamson nanofluid are [26–33], among others.

This current study mainly focuses on the Williamson nanofluid flow past an exponentially stretching surface with a chemical reaction and thermal radiation. This study has many applications in engineering and industrial processes. The Williamson fluid model with a chemical reaction has applications in water and air pollution, atmospheric flows and in chemical engineering problems such as food processes. Thermal radiation has applications in processes such as drying and distribution of temperature and moisture over agricultural fields [34]. Nadeen and Hussain [35] used the homotopy analysis method to explore heat transfer effects on Williamson nanofluid flow over a porous exponentially stretching sheet. The Runge–Kutta–Fehlberg method was used to study the MHD flow of a Williamson nanofluid flow over an exponentially stretching surface by Kumar et al. [34]. Two cases of heat transfer, PEST and PEHF, were investigated on an MHD Williamson nanofluid flow over an exponentially stretching surface by Ahmed and Akbar [36]. Temperature-dependent viscosity and thermal conductivity in a Williamson nanofluid flow over an exponentially stretching sheet were studied by Amjad et al. [37]. Li et al. [38] used MATLAB's bvp4c package to analyze heat and mass transfer in MHD Williamson nanofluid flow over an exponentially porous stretching surface.

Based on the aforementioned studies, it can be noted that there are many studies that have been performed on the Williamson nanofluid flow past an exponentially stretching surface. The novelty of this current study is the addition of thermophoresis and Brownian motion effects in the momentum equation. Additionally, the effects of the magnetic field, thermal radiation, chemical reaction, heat source and injection/suction parameters are simultaneously investigated in this model. The highly non-linear partial differential equations that govern the Williamson nanofluid flow are reduced into non-linear ordinary differential equations using suitable similarity transformations and then solved using the spectral quasi-linearization method (SQLM), developed by Motsa et al. [39]. The effects of some chosen pertinent parameters on the fluid velocity, temperature, concentration, skin friction coefficient, heat transfer rate and mass transfer rate were displayed using graphs and tables. The numerical results obtained in this current research work were validated by comparing the present results with those from MATLAB's bvp4c routine and those results from already-published work. A very good agreement was established.

2. Fluid Model

The Williamson fluid model is used to describe the rheological behaviour of pseudoplastic materials over a wide range of shear stresses and shear rates. The continuity and momentum equations of an incompressible Williamson model are given, respectively, by [40]:

$$div\mathbf{V} = 0, \tag{1}$$

$$\rho_f \frac{d\mathbf{V}}{dt} = div\mathbf{S} + \rho_f \mathbf{b}, \tag{2}$$

where $\frac{d}{dt}$ is the time derivative and $\mathbf{b}$ is the specific body force vector. The Cauchy stress tensor $S = -pI + \tau^*$, [41], where p is the pressure term and I the identity vector. The extra stress tensor is given by:

$$\tau^* = \left(\mu_\infty + \frac{\mu_0 - \mu_\infty}{1 - \Gamma\dot{\gamma}} \right) A_1,$$

where the respective viscosities at zero and infinity shear rate are μ_0 and μ_∞, respectively. The terms A_1 and Γ are the first Revlin–Ericksen tensor and time constant, respectively. Additionally:

$$\dot{\gamma} = \sqrt{\frac{\pi}{2}}, \ \pi = \text{trace}(A_1^2).$$

Choosing $\mu_\infty = 0$ and $\Gamma\dot{\gamma} < 1$ and applying the Binomial expansion, we have the extra stress tensor $\tau^* = \mu_0[1 + \Gamma\dot{\gamma}]A_1$.

3. Mathematical Analysis

Investigated in this current study is a two-dimensional flow of a steady incompressible Williamson nanofluid over a sheet that stretches exponentially. In this flow problem, the coordinate system is chosen in such a way that the x axis is along the stretching sheet and the y axis is measured normal to the sheet. At $y = 0$, the sheet is assumed to be stretching with a velocity $U_w = U_0 e^{\frac{x}{l}}$. The variable magnetic field $B(x) = B_0 e^{\frac{x}{2l}}$ (B_0 is a constant magnetic field) is applied perpendicular to the direction of flow. At the sheet, the fluid has temperature $T_w = T_\infty + T_0 e^{\frac{x}{2l}}$ and nanoparticle fraction $C_w = C_\infty + C_0 e^{\frac{x}{2l}}$. The ambient values of temperature and nanoparticle fraction, far way from the sheet, are denoted by T_∞ and C_∞, respectively. Figure 1 displays the schematic flow diagram and the coordinate system of the problem. Assuming that there is no pressure gradient and applying boundary layer approximations, the continuity, momentum and energy equations governing the flow are given by [25,40]:

$$\frac{\partial u}{\partial x} + \frac{\partial v}{\partial y} = 0, \tag{3}$$

$$u\frac{\partial u}{\partial x} + v\frac{\partial u}{\partial y} = \nu\frac{\partial}{\partial y}\left\{ \frac{\partial u}{\partial y} + \frac{\Gamma}{\sqrt{2}}\left(\frac{\partial u}{\partial y}\right)^2 \right\} + g\beta_T(T - T_\infty) + g\beta_C(C - C_\infty) - \frac{\sigma B^2}{\rho_f}u, \tag{4}$$

$$u\frac{\partial T}{\partial x} + v\frac{\partial T}{\partial y} = \alpha\frac{\partial^2 T}{\partial y^2} + \frac{Q}{(\rho c_p)_f}(T - T_\infty) + \tau\left\{ D_B\frac{\partial T}{\partial y}\frac{\partial C}{\partial y} + \frac{D_T}{T_\infty}\left(\frac{\partial T}{\partial y}\right)^2 \right\}$$

$$-\frac{1}{(\rho c_p)_f}\frac{\partial q_r}{\partial y}, \tag{5}$$

$$u\frac{\partial C}{\partial x} + v\frac{\partial C}{\partial y} = D_B\frac{\partial^2 C}{\partial y^2} + \frac{D_T}{T_\infty}\frac{\partial^2 T}{\partial y^2} - K(C - C_\infty), \tag{6}$$

where u and v are the fluid velocity components in the x and y directions, respectively, ν is the kinematic viscosity of the fluid, g is the acceleration due to gravity, β_T is the thermal

expansion coefficient, β_C is the concentration expansion coefficient, σ is the electrical conductivity, α is thermal diffusivity, $Q(x)(= Q_0 e^{\frac{x}{l}})$ is the variable heat source, ρ_f is the fluid density, D_B is the Brownian diffusion coefficient, D_T is the thermophoresis coefficient, $K(x)(= K_0 e^{\frac{x}{l}})$ is the chemical reaction parameter and $\tau = \frac{(\rho c_p)_p}{(\rho c_p)_f}$ is the ratio of the effective heat capacity of the nanoparticle material and heat capacity of the fluid.
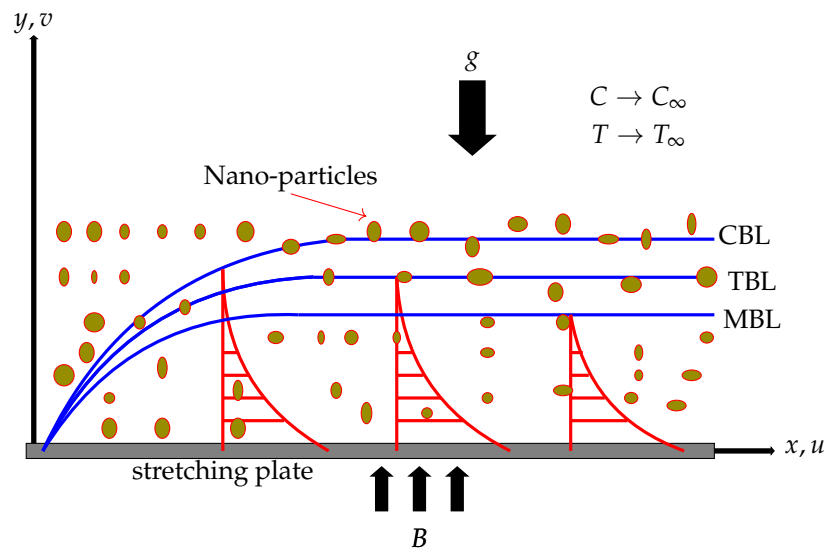
C/T/MBL - Concentration/Thermal/Momentum Boundary Layer

Figure 1. Schematic flow diagram and coordinate system.

The energy Equation (5) can be simplified by using the Rosseland approximation [42], which states that the radiative heat flux:

$$q_r = \frac{4\sigma^*}{3k^*}\frac{\partial T^4}{\partial y},$$

where σ^* is the Stefan–Boltzmann constant and k^* is the mean absorption coefficient. Assuming that the temperature differences within the flow are so small, the linear Taylor series expansion of T^4 about T_∞ gives $T^4 \approx 4TT_\infty^3 - 3T_\infty^3$ such that:

$$\frac{\partial q_r}{\partial y} = -\frac{16\sigma^* T_\infty^3}{3k^*}\frac{\partial^2 T}{\partial y^2}. \tag{7}$$

Using Equation (7) in Equation (5) gives:

$$u\frac{\partial T}{\partial x} + v\frac{\partial T}{\partial y} = \left(\alpha + \frac{16\sigma^* T_\infty^3}{3(\rho c_p)_f k^*}\right)\frac{\partial^2 T}{\partial y^2} + \frac{Q}{(\rho c_p)_f}(T - T_\infty) + \tau\left\{D_B\frac{\partial T}{\partial y}\frac{\partial C}{\partial y} + \frac{D_T}{T_\infty}\left(\frac{\partial T}{\partial y}\right)^2\right\}, \tag{8}$$

The suitable boundary conditions for the system of Equations (3)–(6) are:

$$\begin{aligned} u = U_w = U_0 e^{\frac{x}{l}}, \ v = -\gamma(x), \ \text{where } \gamma(x) = -V_0 e^{\frac{x}{2l}}, \\ T = T_w = T_\infty + T_0 e^{\frac{x}{2l}}, \ C = C_w = C_\infty + C_0 e^{\frac{x}{2l}}, \ \text{at } y = 0, \\ u \to 0, \ T \to T_\infty, \ C \to C_\infty, \ \text{as } y \to \infty. \end{aligned} \tag{9}$$

The similarity transformations which are used to solve the governing equations are defined as follows [43]:

$$u = U_0 e^{\frac{x}{l}} f'(\eta), \; v = -\sqrt{\frac{\nu U_0}{2l}} e^{\frac{x}{2l}} [f(\eta) + \eta f'(\eta)], \; \eta = \sqrt{\frac{U_0}{2\nu l}} y e^{\frac{x}{2l}},$$

$$T = T_\infty + T_0 e^{\frac{x}{2l}} \theta(\eta), \; C = C_\infty + C_0 e^{\frac{x}{2l}} \phi(\eta) \tag{10}$$

Using similarity transformations Equation (10), the continuity Equation (3) is identically satisfied and Equations (4)–(6) take the following form:

$$f''' + ff'' - 2f'^2 + \lambda f'' f''' - M^2 f' + 2G_T \theta + 2G_C \phi = 0, \tag{11}$$

$$\left(1 + \frac{4}{3} R_d\right) \theta'' + Pr(f\theta' - f'\theta + N_b \phi'\theta' + N_t \theta'^2 + \delta\theta) = 0, \tag{12}$$

$$\phi'' + Sc(f\phi' - f'\phi - K_r\phi) + \frac{N_t}{N_b}\theta'' = 0, \tag{13}$$

subject to boundary conditions:

$$f(0) = -S, \; f'(0) = 1, \; \theta(0) = 1, \; \phi(0) = 1,$$
$$f'(\infty) \to 0, \; \theta(\infty) \to 0, \; \phi(\infty) \to 0. \tag{14}$$

where $\lambda \left(= \Gamma \sqrt{\frac{U_0^3 e^{\frac{3x}{l}}}{\nu l}}\right)$ is the Williamson fluid parameter, $M^2 (= \frac{2l\sigma B_0^2}{\rho U_0})$ is the magnetic field parameter, $G_T (= \frac{glB_T T_0}{U_0^2})$ is the thermal Grashof number, $G_C (= \frac{glB_C C_0}{U_0^2})$ is the mass Grashof number, $Pr (= \frac{\nu}{\alpha})$ is the Prandlt number, $R_d (= \frac{4\sigma^* T_\infty^3}{k^* \kappa})$ is the radiation parameter, $N_b (= \frac{\tau D_B}{\nu}(C_w - C_\infty))$ is the Brownian motion parameter, $N_t (= \frac{\tau D_T}{\nu T_\infty}(T_w - T_\infty))$ is the thermophoresis parameter, $\delta (= \frac{2lQ_0}{\rho c_p U_0})$ is the heat generation parameter, $Sc (= \frac{\nu}{D_B})$ is the Schmidt number, $S (= V_0 \sqrt{\frac{2l}{\nu U_0}})$ is the suction $(S < 0)$ or the injection $(S > 0)$ parameter and $K_r (= \frac{2lK_0}{U_0})$ is the chemical reaction parameter.

The skin friction coefficient (c_f), the local Nusselt number (Nu_x) and the local Sherwood number (Sh_x) are the physical quantities of engineering significance discussed in this study. Following the work by Ahmed and Akbar [36]:

$$c_f = \frac{1}{\rho U_w^2} \left(\mu \left(\frac{\partial u}{\partial y} + \frac{\Gamma}{\sqrt{2}}\left(\frac{\partial u}{\partial y}\right)^2\right)\right)_{y=0},$$

$$Nu_x = -\frac{\sqrt{2}l}{(T_w - T_\infty)e^{\frac{x}{2l}}}\left(\frac{\partial T}{\partial y}\right)_{y=0},$$

$$Sh_x = -\frac{\sqrt{2}l}{(C_w - C_\infty)e^{\frac{x}{2l}}}\left(\frac{\partial C}{\partial y}\right)_{y=0}.$$

Using similarity transformations in Equation (10), the following dimensionless forms are obtained:

$$\sqrt{2Re_x}c_f = \left(f''(0) + \frac{\lambda}{2}(f''(0))^2\right),$$

$$\frac{Nu_x}{\sqrt{Re_x}} = -\theta'(0), \; \frac{Sh_x}{\sqrt{Re_x}} = -\phi'(0),$$

where $Re_x = \frac{U_w l}{\nu}$ is the Reynolds number.

4. Method of Solution

In this study, the spectral quasi-linearization method is used to seek the numerical solution of the coupled system of Equations (11)–(13) subject to boundary conditions Equation (18). A Newton–Raphson-based quasi-linearization method [44], which uses first-order Taylor series expansion, is used to linearize the non-linear terms. Denote the respective solutions of Equations (11)–(13) at iteration level s by f_s, θ_s and ϕ_s, respectively. Assuming that the difference between solutions at iteration level s and $s+1$ are sufficiently close, quasi-linearization gives the following iterative sequence of linear differential equations:

$$a_{0,s}f'''_{s+1} + a_{1,s}f''_{s+1} + a_{2,s}f'_{s+1} + a_{3,s}f_{s+1} + a_{4,s}\theta_{s+1} + a_{5,s}\phi_{s+1} = R_{1,s}, \tag{15}$$

$$b_{0,s}\theta''_{s+1} + b_{1,s}\theta''_{s+1} + b_{2,s}\theta_{s+1} + b_{3,s}f'_{s+1} + b_{4,s}f_{s+1} + b_{5,s}\phi'_{s+1} = R_{2,s}, \tag{16}$$

$$c_{0,s}\phi''_{s+1} + c_{1,s}\phi'_{s+1} + c_{2,s}\phi_{s+1} + c_{3,s}f'_{s+1} + c_{4,s}f_{s+1} + c_{5,s}\theta''_{s+1} = R_{3,s}, \tag{17}$$

where the variable coefficients known at iteration level s are defined as:

$$a_{0,s} = 1 + \lambda f''_s, \ a_{1,s} = f_s + \lambda f'''_s, \ a_{2,s} = -4f'_s - M, \ a_{3,s} = f''_s, \ a_{4,s} = 2G_T, \ a_{5,s} = 2G_C,$$

$$b_{0,s} = 1 + \frac{4}{3}R_d, \ b_{1,s} = Pr(f_s + N_b\phi'_s + 2N_t\theta'_s), \ b_{2,s} = -Pr(f'_s - \delta), \ b_{3,s} = -Pr\theta_s,$$

$$b_{4,s} = Pr\theta'_s, \ b_{5,s} = PrN_b\theta'_s, \ c_{0,s} = 1, \ c_{1,s} = Scf_s, \ c_{2,s} = -Sc(f'_s + K_r),$$

$$c_{3,s} = -Sc\phi_s, \ c_{4,s} = Sc\phi'_s, \ c_{5,s} = \frac{N_t}{N_b}.$$

The boundary conditions given in Equation (18) are transformed to:

$$f'_{s+1}(0) = 1, \ f_{s+1}(0) = -S, \ \theta_{s+1}(0) = 1, \ \phi_{s+1}(0) = 1,$$

$$f'_{s+1}(\infty) \to 0, \ \theta_{s+1}(\infty) \to 0, \ \theta_{s+1}(\infty) \to 0. \tag{18}$$

The terms on the right hand side are:

$$R_{1,s} = f_s f''_s - 2f'^2_s + \lambda f''_s f'''_s, \ R_{2,s} = Pr(f_s\theta'_s - f'_s\theta + N_b\theta'_s\phi'_s + N_t\theta'^2_s),$$

$$R_{3,s} = Sc(f_s\phi'_s - f'_s\phi_s)$$

The unknown functions f_{s+1}, θ_{s+1} and ϕ_{s+1} are approximated using Chebyshev interpolating polynomials, such that the their derivatives evaluated at Gauss–Lobatto collocation points $\eta_i = \cos\frac{\pi i}{N} (i = 0, 1, 2, \cdots, N)$ are given by:

$$\frac{d^n f_{s+1}}{d\eta}(\eta_i) = \sum_{k=0}^{N} D^n_{ik}f_{s+1}(\eta_k) = \mathbf{D}^n\mathbf{F}_{s+1},$$

$$\frac{d^n \theta_{s+1}}{d\eta}(\eta_i) = \sum_{k=0}^{N} D^n_{ik}\theta_{s+1}(\eta_k) = \mathbf{D}^n\mathbf{\Theta}_{s+1}, \tag{19}$$

$$\frac{d^n \phi_{s+1}}{d\eta}(\eta_i) = \sum_{k=0}^{N} D^n_{ik}\phi_{s+1}(\eta_k) = \mathbf{D}^n\mathbf{\Phi}_{s+1},$$

where

$\mathbf{D} = \frac{2}{L_\infty}D$, $\mathbf{F}_{s+1} = [f_{s+1}(\eta_0), f_{s+1}(\eta_1), \cdots, f_{s+1}(\eta_{N-1}), f_{s+1}(\eta_N)]^T$,

$\mathbf{\Theta}_{s+1} = [\theta_{s+1}(\eta_0), \theta_{s+1}(\eta_1), \cdots, \theta_{s+1}(\eta_{N-1}), \theta_{s+1}(\eta_N)]^T$,

$\mathbf{\Phi}_{s+1} = [\phi_{s+1}(\eta_0), \phi_{s+1}(\eta_1), \cdots, \phi_{s+1}(\eta_{N-1}), \phi_{s+1}(\eta_N)]^T$.

Using derivatives in Equation (19) in the system of Equations (15)–(17) yields a system in vector matrix form:

$$\begin{bmatrix} \mathbf{A11} & \mathbf{A12} & \mathbf{A13} \\ \mathbf{A21} & \mathbf{A22} & \mathbf{A23} \\ \mathbf{A31} & \mathbf{A32} & \mathbf{A33} \end{bmatrix} \begin{bmatrix} \mathbf{F}_{s+1} \\ \mathbf{\Theta}_{s+1} \\ \mathbf{\Phi}_{s+1} \end{bmatrix} = \begin{bmatrix} \mathbf{R}_{1,s} \\ \mathbf{R}_{2,s} \\ \mathbf{R}_{3,s} \end{bmatrix},$$

where

$$\mathbf{A}11 = \mathbf{a}_{0,s}\mathbf{D}^3 + \mathbf{a}_{1,s}\mathbf{D}^2 + \mathbf{a}_{2,s}\mathbf{D} + \mathbf{a}_{3,s}, \ \mathbf{A}12 = a_{4,s}\mathbf{I}, \ \mathbf{A}13 = a_{5,s}\mathbf{I},$$
$$\mathbf{A}21 = \mathbf{b}_{3,s}\mathbf{D} + \mathbf{b}_{4,s}, \ \mathbf{A}22 = b_{0,s}\mathbf{D}^2 + \mathbf{b}_{1,s}\mathbf{D} + \mathbf{b}_{2,s}, \ \mathbf{A}23 = \mathbf{b}_{5,s}\mathbf{D},$$
$$\mathbf{A}31 = \mathbf{c}_{3,s}\mathbf{D} + \mathbf{c}_{4,s}, \ \mathbf{A}32 = c_{5,s}\mathbf{D}^2, \ \mathbf{A}33 = c_{0,s}\mathbf{D}^2 + \mathbf{c}_{1,s}\mathbf{D} + \mathbf{c}_{2,s}.$$

where $\mathbf{I}$ is an $(N+1) \times (N+1)$ identity matrix. The spectral boundary conditions are:

$$f_{s+1}(\eta_N) = S, \ \sum_{k=0}^{N} D_{N,k}f_{s+1}(\eta_N) = 1, \ \theta_{s+1}(\eta_N) = 1, \ \phi_{s+1}(\eta_N) = 1,$$

$$\sum_{k=0}^{N} D_{0,k}f_{s+1}(\eta_0) = 0, \ \theta_{s+1}(\eta_0) = 0, \ \phi_{s+1}(\eta_0) = 0.$$

The numerical iteration of the SQLM, coded in MATLAB R2022b on an Intel(R) Core(TM) i5, is started by using the initial guesses that satisfy the boundary conditions Equation (18), given by:

$$f_0(\eta) = 1 - e^{-\eta} + S, \ \theta_0(\eta) = e^{-\eta}, \ \phi_0(\eta) = e^{-\eta}.$$

5. Results and Discussion

5.1. Validation of Results

To confirm the accuracy of the SQLM used in this study, the values of the skin friction $-(f''(0) + \frac{\lambda}{2}(f''(0))^2)$ are compared against the MATLAB bvp4c solver results and the homotopy analysis method results obtained by Nadeem and Hussain [40] and Amjad et al. [45]. Considering the values $G_T = G_C = 0$, Equation (11) reduces to the problem by Amjad et al. [45], which is given by:

$$f''' + ff'' - 2f'^2 + \lambda f''f''' - M^2 f' = 0, \tag{20}$$

subject to boundary conditions:

$$f(0) = -S, \ f'(0) = 1, \ f'(\infty) \to 0. \tag{21}$$

Using $N = 40$ collocation points, $\eta_\infty = 5.0$, the MATLAB SQLM algorithm for solving Equation (20) involves iteratively solving the following recursive sequence:

$$\begin{bmatrix} D_{0,0} & D_{0,1} & \cdots & D_{0,N-1,} & D_{0,N} \\ & & \mathbf{A} & & \\ D_{N,0} & D_{N,1} & \cdots & D_{N,N-1} & D_{N,N} \\ 0 & 0 & \cdots & & 1 \end{bmatrix} \begin{bmatrix} f_{s+1}(\eta_0) \\ \mathbf{F}_{s+1} \\ f_{s+1}(\eta_{N-1}) \\ f_{s+1}(\eta_N) \end{bmatrix} = \begin{bmatrix} 0 \\ \mathbf{R}_s \\ 1 \\ -S \end{bmatrix}, \tag{22}$$

where $\mathbf{A} = \mathbf{a}_{0,s}\mathbf{D}^3 + \mathbf{a}_{1,s}\mathbf{D}^2 + \mathbf{a}_{2,s}\mathbf{D} + \mathbf{a}_{3,s}$, $\mathbf{F}_{s+1} = [f_{s+1}(\eta_1), f_{s+1}(\eta_2), \cdots, f_{s+1}(\eta_{N-3}),$ $f_{s+1}(\eta_{N-2})]^T$ and $\mathbf{R}_s = -2\mathbf{F}'_s \circ \mathbf{F}'_s + \mathbf{F}_s \circ \mathbf{F}''_s) + \lambda \mathbf{F}''_s \circ \mathbf{F}'''_s$. Performing 20 iterations, the results obtained for $-(f''(0) + \frac{\lambda}{2}(f''(0))^2)$ are displayed in Table 1.

Table 1 displays the computed values of the skin friction coefficient compared against the results by Amjad et al. [45] for different values of λ, S and M. A good match of the results is observed. The accuracy of the SQLM was validated by a direct comparison with the reported results.

Considering $G_T = G_C = 0 = M = 0$, Equation (11) reduces to the problem by Nadeem and Hussain [40], which can be solved using MATLAB's bvp4c solver by first using the following substitutions:

$$y(1) = f, \ y(2) = f', \ y(3) = f'' \tag{23}$$

$$f''' = y(3)' = \frac{2(y(2))^2 - y(1)y(3)}{(1 + \lambda y(3))} \tag{24}$$

and the boundary conditions are given as $y_a(1) + S$, $y_a(2) - 1$, $y_b(2)$. The three first-order equations are coded in the MATLAB's bvp4c solver with the function name "odeBVP", and with "odeBc" handling the boundary conditions. Choosing the interval of integration to $[0, 40]$, the solutions from the function "bvp4c" are given by:

```
sol = bvp4c(@odeBVP, @odeBc, solinit, options).
```

A comparison of the SQLM skin friction coefficient values against those from MATLAB's bvp4c routine and the results by Nadeem and Hussain [40] is shown in Table 2. A perfect agreement was observed.

Table 1. Table of present values of $\sqrt{2Re}C_f$ compared against published results for varying values of λ, S and M.

			$-(f''(0) + \frac{\lambda}{2}(f''(0))^2)$	
λ	**S**	**M**	**Amjad et al. [45]**	**SQLM**
0.1	0.2	2.0	1.754213	1.754213105760364
0.2	0.2	2.0	1.678675	1.678675073146794
0.3	0.2	2.0	1.579827	1.578533717157394
0.1	0.1	2.0	1.799249	1.799249869955796
0.1	0.2	2.0	1.754213	1.754213105760364
0.1	0.3	2.0	1.710489	1.710489423953702
0.1	0.2	0.1	1.201556	1.201559983439274
0.1	0.2	0.2	1.237223	1.237224345281889
0.1	0.2	0.3	1.271816	1.271816653083256

Table 2. Table of present values of $\sqrt{2Re}C_f$ compared against MATLAB's bvp4c results for selected values of λ and $S = 0.1$.

	$-(f''(0) + \frac{\lambda}{2}(f''(0))^2)$		
λ	**Nadeem and Hussain [40]**	**MATLAB's bvp4c**	**SQLM**
0.0	1.32930	1.329302736062721	1.329308462412963
0.1	1.29801	1.298017071294807	1.298022829158239
0.2	1.26310	1.263103796098337	1.263109548733657
0.3	1.22276	1.222776617114427	1.222781418705920

5.2. Results

The SQLM algorithm was implemented using MATLAB R2022b software. For all the numerical results, unless otherwise stated, the default parameters considered are: $N = 60$, $M = 0.1$, $G_T = 0.1$, $\lambda = 0.3$, $G_C = 0.1$, $N_t = 0.1$, $N_b = 0.1$, $Pr = 0.5$, $\delta = 0.2$, $S = 0.0$, $Kr = 0.1$, $Sc = 1.0$. The convergence and accuracy of the spectral quasi-linearization method were verified using the solution error norms and residual errors, respectively. The solution error norms, defined as the difference between values of successive iterations are denoted by [46]:

$$Err[F(\eta)] = ||F_{s+1}(\eta) - F_s(\eta)||_\infty, \ Err[\Theta(\eta)] = ||\Theta_{s+1}(\eta) - \Theta_s(\eta)||_\infty, \ Err[\Phi(\eta)] = ||\Phi_{s+1}(\eta) - \Phi_s(\eta)||_\infty.$$

The residual error gives a measure of the extent to which the SQLM solution approximates the true solution. The residual L^∞ norms are given by Alharbey et al. [47] as:

$$Res(f) = ||f''' + ff'' - 2f'^2 + \lambda f'' f''' - M^2 f' + 2G_T \theta + 2G_C \phi||_\infty,$$
$$Res(\theta) = ||(1 + (4/3)R_d \theta'' + Pr(f\theta' - f'\theta + N_b \phi'\theta' + N_t \theta'^2 + \delta\theta))||_\infty,$$
$$Res(\phi) = ||\phi'' + Sc(f\phi' - f'\phi - Kr\phi) + (N_t/N_b)\theta''||_\infty,$$

Figure 2a reveals that the SQLM converges after only five iterations with a solution based error of order $\approx 10^{-10}$. Additionally, after three iterations, the SQLM achieves an accuracy of order $\approx 10^{-9}$, as shown in Figure 2b.
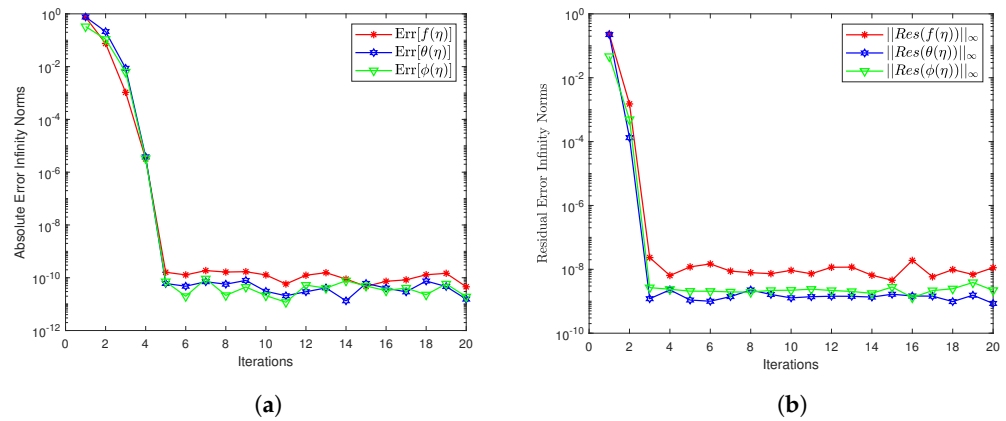

(**a**)

(**b**)

Figure 2. Error graphs of $f(\eta)$, $\theta(\eta)$ and $\phi(\eta)$.

Figures 3–5 display the effects of the magnetic parameter (M), suction/injection parameter (S) and the Williamson parameter (λ), respectively, on the fluid velocity profiles. Figure 3 shows that the fluid velocity is depressed as the magnetic parameter is increased. Physically, the fluid velocity drops due to the resistive Lorentz force, which is induced by the magnetic parameter. It is depicted in Figure 4 that the Williamson nanofluid velocity profiles are depressed when the suction parameter is increased. Additionally, it is revealed in Figure 5 that there is an inverse relationship between the fluid velocity distribution and the non-Newtonian Williamson parameter. An increase in the values of λ causes a decrease in the fluid movement and reduces the boundary layer thickness.
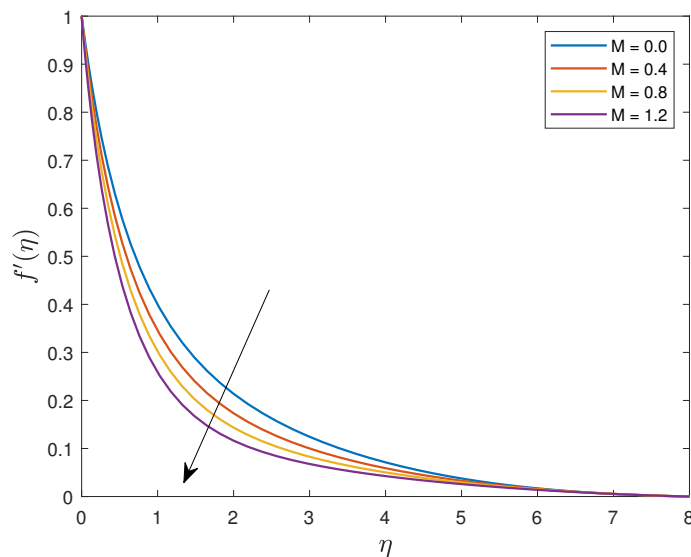

Figure 3. Influence of M on the nanofluid velocity.

The influences of the Prandtl number (Pr), Brownian motion parameter (N_b), thermal Grashof parameter (G_T) and thermal radiation parameter (R_d) on the Williamson nanofluid dimensionless temperature (θ) are depicted in Figures 6–9, respectively. It is displayed in Figure 6 that the fluid temperature and thermal boundary layer are reduced as the Prandtl number increases. The Prandtl number can be viewed as the ratio of momentum to thermal boundary layers. Physically, a high Prandtl number means a small thermal boundary layer. It is revealed in Figure 7 that an increase in the values of the Brownian motion

parameter increases the fluid temperature profile. An increase in the Brownian motion parameter results in an increased kinetic energy of the Williamson nanoparticles, and hence, a temperature increase. Figure 8 depicts that the fluid temperature is depressed as the thermal Grashof number is enhanced. Essentially, the Grashof number signifies the ratio of buoyancy to viscous forces. Increasing G_T results in an addition of more thermal energy in the fluid molecules, which in turn increases the fluid local heat transfer rate. The thermal boundary layer is reduced, and hence, the temperature profiles decrease. It is shown in Figure 9 that temperature is an increasing function of the thermal radiation parameter. The effect of increasing the thermal radiation parameter is thickening the thermal boundary layer, and hence, the temperature profiles are increased.
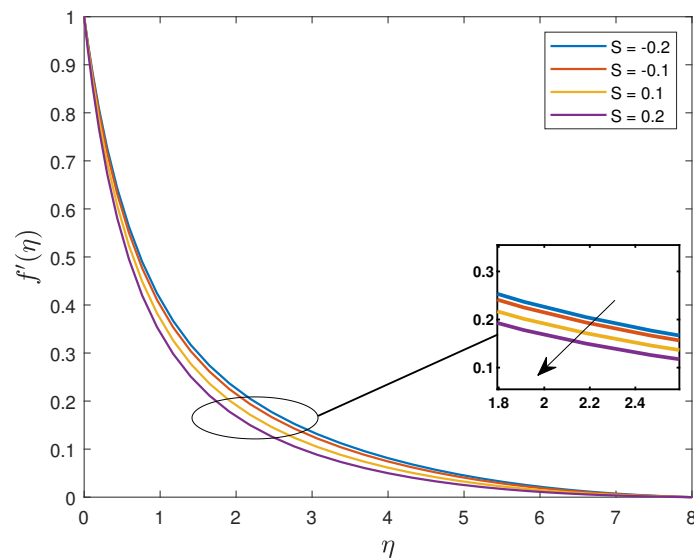

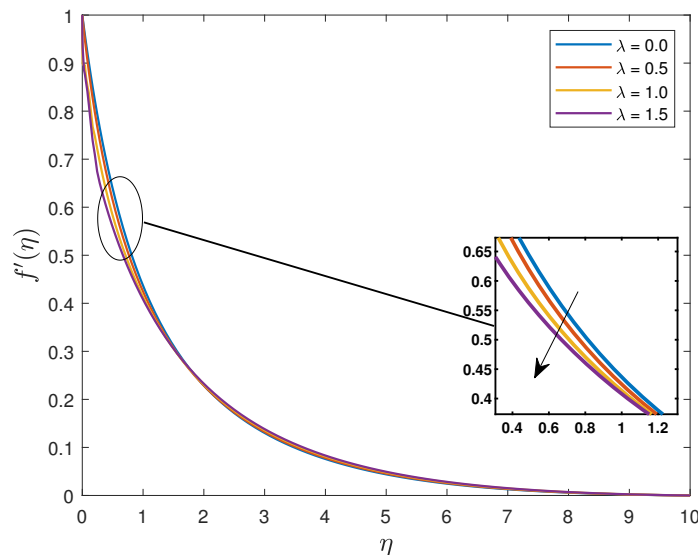**Figure 4.** Influence of S on the nanofluid velocity.

Figure 5. Influence of λ on fluid velocity.

Figure 10 portrays the influence of the Schmidt number (Sc) on the Williamson nanoparticle concentration. *Sc* can be defined as the ratio of momentum diffusivity and mass diffusivity. High values of *Sc* corresponds to a weaker solute diffusivity and the concentration distribution and solute boundary layer decrease as a consequence. The fluid dimensionless concentration profiles are depressed when the chemical reaction parameter is increased as seen in Figure 11. Physically, when the chemical reaction parameter is increased, quite a

number of solute molecules will undergo chemical reaction, and hence, the reduction in the concentration. The influence of the mass Grashof number (G_C) on the concentration is displayed in Figure 12. G_C relates species buoyancy force to the viscous hydrodynamic force. Increasing G_C causes an enhancement of the concentration gradient, which in turn boosts the buoyancy effect. A resulting induced flow will cause a decrease in concentration, and hence, a decrease in the concentration profile, as depicted in Figure 12.
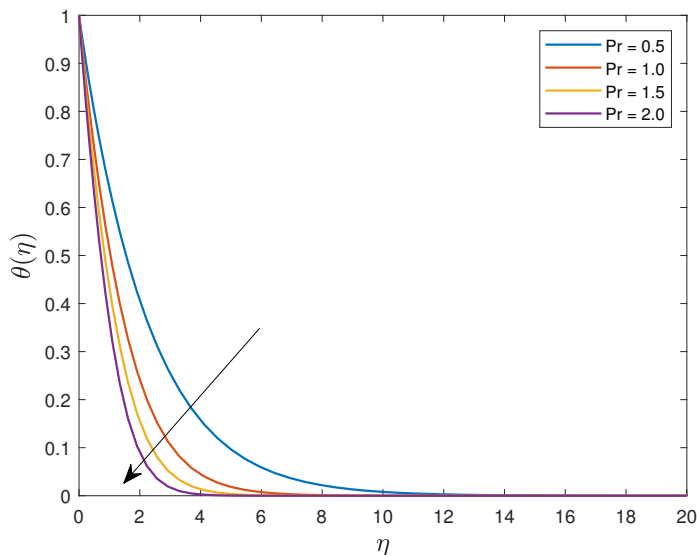

Figure 6. Influence of *Pr* on fluid temperature.
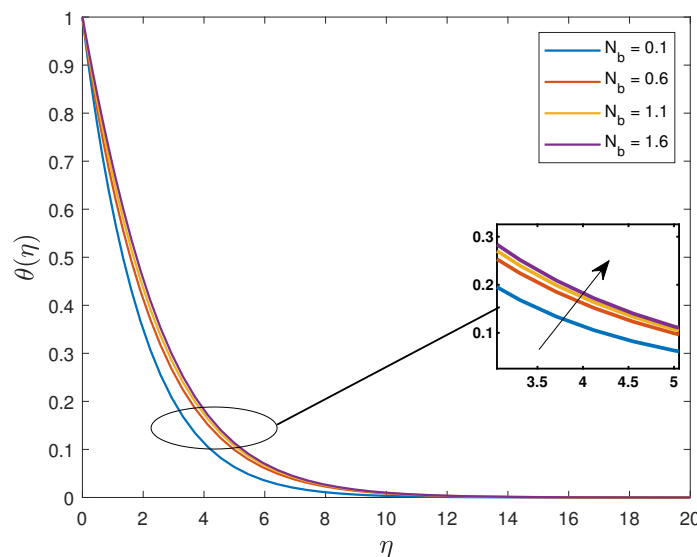

Figure 7. Influence of N_b on fluid temperature.

Table 3 displays the effects of all the pertinent thermo-physical parameters involved in the current problem on the skin friction, Nusselt number and Sherwood number. The skin friction coefficient upsurges as the values of injection parameter, Prandtl number, magnetic parameter, Brownian motion parameter and Schmidt number are increased. The fluid flow is improved by the functioning magnetic field regarding the Williamson nanofluid, and thus, increases the surface friction. The increase of $\sqrt{2Re}C_f$ with an increasing Prandtl number is attributed to increased fluid momentum. The opposite trend is observed when the Williamson fluid parameter, mass Grashof number, thermal Grashof number, thermal radiation parameter, thermophoresis parameter, heat generation parameter and chemical reaction parameter are increased.
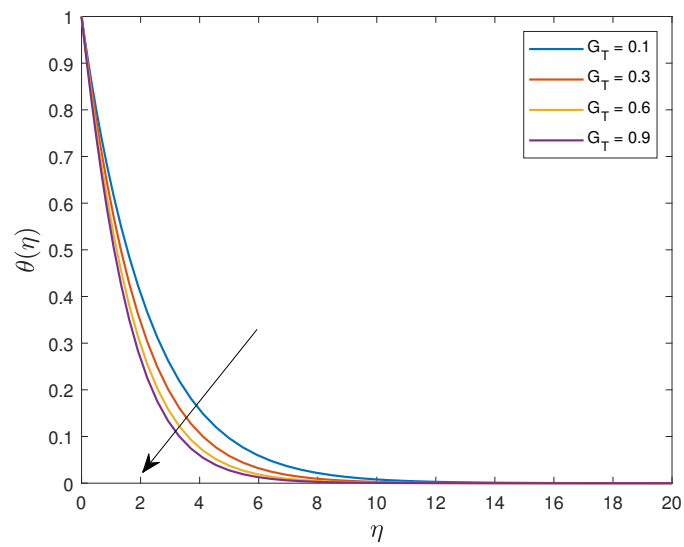
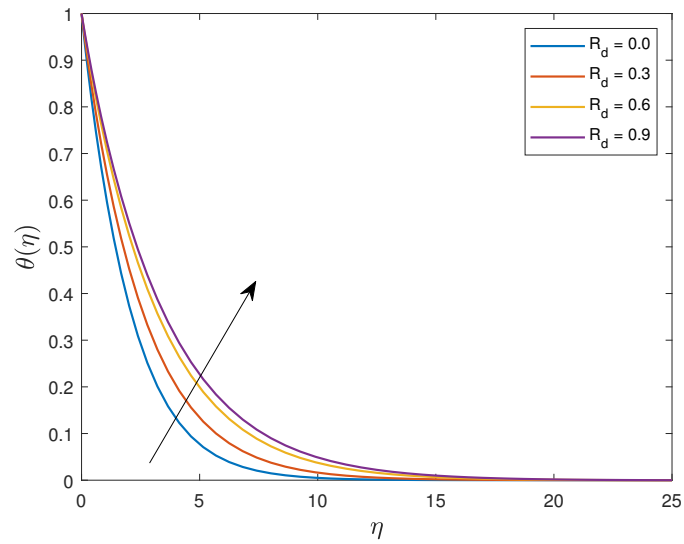**Figure 8.** Influence of G_T on fluid temperature.
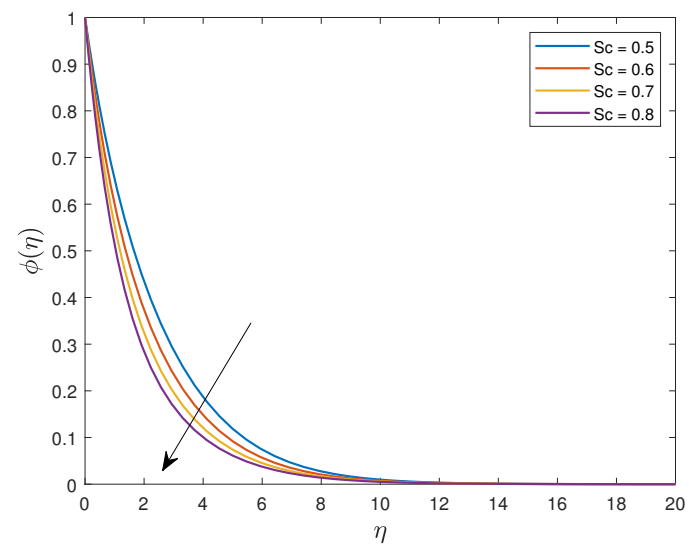

Figure 9. Influence of R_d on fluid temperature.

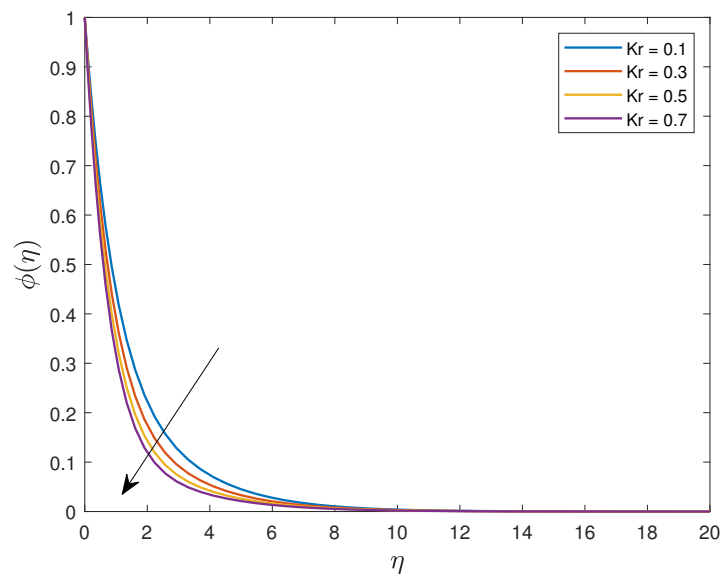**Figure 10.** Influence of Sc on fluid concentration.

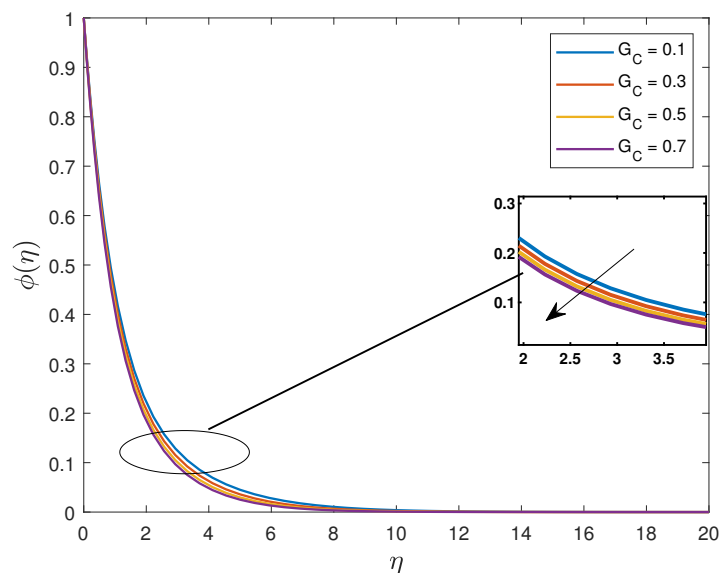**Figure 11.** Influence of *Kr* on fluid concentration.

Figure 12. Influence of *Gc* on fluid concentration.

It is also noted that the mass Grashof number and the thermal Grashof number are the only parameters whose increment enhances the Nusselt number. Increasing the values of the Williamson fluid parameter, injection parameter, magnetic parameter, Prandtl number, thermal radiation, Brownian motion parameter, thermophoresis parameter, heat generation parameter, Schmidt number and chemical reaction parameter suppresses the heat transfer rate. It is noted that Nusselt number is a decreasing function of N_b and N_t. Physically, the effects of both Brownian motion and themorphoresis effects move the Williamson nanoparticles away from the stretching sheet sheet, intensifying the the diffusion of the nanoparticles into the boundary layer, and hence, causing a decrease in the Nusselt number.

The Sherwood number is improved as the values of mass Grashof number, thermal Grashof number, thermal radiation parameter, Brownian motion parameter, heat generation parameter, Schmidt number and chemical reaction parameter are increased and depreciates as the Williamson fluid parameter, injection parameter, magnetic parameter, Prandtl number and thermophoresis parameter are increased. The Schmidt number is the relative effectiveness of the momentum and mass transport by diffusion in the hydrodynamic and species boundary layers. An increase in *Sc* will result in an increase in the Sherwood

number. An increased chemical reaction parameter means there will be more interaction of species concentration with the momentum boundary, and hence, an increase in the Sherwood number.

Table 3. The numerical values of the skin friction coefficient, Nusselt number and Sherwood number for all the thermo-physical parameters.

λ	S	M	Pr	G_C	G_T	R_d	N_b	N_t	δ	Sc	Kr	$\sqrt{2Re}\,C_f$	$-\frac{Nu_x}{\sqrt{Re_x}}$	$-\frac{Sh_x}{\sqrt{Re_x}}$
0.1	0.2	2.0	0.5	0.1	0.1	0.1	0.5	0.5	0.1	1.0	0.1	1.776767	0.308282	0.700530
0.3												1.706494	0.295463	0.687057
0.9												1.608996	0.169515	0.539204
0.1	0.1											1.730004	0.323907	0.736618
	0.2											1.776768	0.308282	0.700530
	0.3											1.824988	0.294009	0.665454
	0.2	0.1										1.174219	0.434167	0.794308
		0.2										1.213171	0.426083	0.787275
		0.3										1.251027	0.418169	0.780543
		2.0	0.1									1.771939	0.147223	0.810761
			0.2									1.773217	0.191519	0.780377
			0.3									1.774461	0.233031	0.751949
			0.5	0.3								1.635586	0.347227	0.724385
				0.6								1.430563	0.391337	0.757335
				0.9								1.232356	0.424697	0.786362
				0.1	0.3							1.474263	0.368464	0.735159
					0.6							1.246002	0.419482	0.777179
					0.9							1.027907	0.454621	0.811112
					0.1	0.3						1.470957	0.273691	0.724148
						0.5						1.468421	0.248889	0.741101
						0.7						1.466412	0.230255	0.753849
						0.1	0.1					1.390481	0.316343	0.032976
							0.3					1.461652	0.312301	0.593189
							0.5					1.474263	0.308282	0.700530
							0.5	0.1				1.491310	0.358320	0.807764
								0.3				1.482646	0.324544	0.753061
								0.5				1.474263	0.308282	0.700530
								0.1	0.0			1.477366	0.382548	0.658192
									0.1			1.474263	0.308282	0.700530
									0.2			1.470240	0.198753	0.756672
									0.1	0.6		1.446575	0.322304	0.458305
										0.8		1.461864	0.314201	0.587691
										1.0		1.474263	0.308282	0.700530
										1.0	0.2	1.479727	0.303787	0.778334
											0.4	1.488552	0.297958	0.906974
											0.6	1.495533	0.294169	1.015232

6. Conclusions

In this manuscript, the spectral quasi-linearization method was applied to numerically analyze the magnetoxhydrodynamics Williamson nanofluid flow over an exponentially stretching surface with chemical reaction and thermal radiation nanofluid flow. A comparison of the skin friction coefficient results obtained from MATLAB's bvp4c solver and published work confirmed that the method is reliable for solving the current problem. The key findings from the study are as follows:

1. The dimensionless velocity ($f'(\eta)$) diminishes as the values of the magnetic parameter are increased from 0 to 1.2;
2. The dimensionless temperature ($\theta(\eta)$) is an increasing function of $0.1 \leq N_b \leq 1.6$ and $0.0 \leq R_d \leq 0.9$;
3. The dimensionless concentration ($\phi(\eta)$) decreases for $0.5 \leq Sc \leq 0.8$ and $0.1 \leq Kr \leq 0.7$;
4. The skin friction coefficient increases as $M(0.1 \leq M \leq 0.3)$ and $N_b(0.1 \leq N_b \leq 0.5)$ increase and depressed for increased values of $N_t(0.1 \leq N_t \leq 0.5)$;
5. The Nusselt number diminishes as $M(0.1 \leq M \leq 0.3)$, $N_b(0.1 \leq N_b \leq 0.5)$ and $N_t(0.1 \leq N_t \leq 0.5)$ are increased;
6. The Sherwood number decreases as $M(0.1 \leq M \leq 0.3)$ and $N_t(0.1 \leq N_t \leq 0.37)$ increase and decreases as $N_b(0.3 \leq N_b \leq 0.7)$ increases.

Nomenclature

x, y	Cartesian coordinates [m]
u, v	Velocity components in the x and y directions, respectively [m s^{-1}]
U_0	Reference velocity [m s^{-1}]
β_T	Thermal expansion coefficient
β_C	Concentration expansion coefficient
B_0	Magnetic field strength [NmA^{-1}]
C_f	Skin friction coefficient
Pr	Prandtl number
M	Magnetic parameter [Te]
T	Fluid temperature [T]
C_w	Concentration of nanoparticles at the surface [mol m^{-3}]
C	Concentration of nanoparticles [mol m^{-3}]
U_w	Velocity at the wall [m s^{-1}]
Q	Heat source
K_r	Chemical reaction parameter [Ms^{-1}]
T_0	Reference temperature [K]
C_0	Reference concentration [mol m^{-3}]
R_d	Thermal radiation parameter
q_r	Radiative heat flux [J]
S	Suction/injection parameter
$\theta(\eta)$	Dimensionless temperature
$\phi(\eta)$	Dimensionless concentration
N_t	Thermophoretic parameter
Nu_x	Local Nusselt number
Sh_x	Local Sherwood number
T_w	Surface temperature [K]
T_∞	Ambient temperature [K]
f	Dimensionless stream function
g	Acceleration due to gravity [m s^{-2}]
Sc	Schmidt number
D_B	Brownian diffusion coefficient [m^2 s^{-1}]

D_T	Thermophoresis diffusion coefficient [m^2 s^{-1}]
μ_∞	Infinite viscosity [Nsm^{-2}]
$(\rho c_p)_f$	Heat capacity of the nanofluid [Jm^{-3}K^{-1}]
Re_x	Reynolds number
$f'(\eta)$	Velocity profile
η	Dimensionless similarity variable
σ	Electrical conductivity [Sm^{-1}]
Γ	Positive time constant
α	Thermal diffusivity [m^{-2} s^{-1}]
$(\rho c_p)_p$	Heat capacity of the nanoparticles [Jm^{-3} K^{-1}]
ν	Kinematic viscosity [m^2 s^{-1}]
ρ_f	Fluid density [kg m^{-3}]
λ	Williamson fluid parameter
Gr_T	Thermal Grashof number
Gr_C	Concentration Grashof number

References

1. Matsuhisa, S.; Bird, R.B. Analytical and numerical solutions for laminar flow of the non-Newtonian ellis fluid. *AIChE J.* **1965**, *11*, 588–595. [CrossRef]
2. Carreau, P.J. Rheological Equations from Molecular Network Theories. *Trans. Soc. Rheol.* **1972**, *16*, 99–127. 10.1122/1.549276. [CrossRef]
3. Ostwald, W. Ueber die rechnerische Darstellung des Strukturgebietes der Viskosität. *Kolloid Z.* **1929**, *47*, 176–187. [CrossRef]
4. Cross, M.M. Rheology of non-Newtonian fluids: A new flow equation for pseudoplastic systems. *J. Colloid Sci.* **1965**, *20*, 417–437. [CrossRef]
5. Casson, N. A Flow Equation for Pigment-Oil Suspensions of the Printing Ink Type. In *Rheology of Disperse Systems*; Mill, C.C., Ed.; Pergamon Press: Oxford, UK, 1959; pp. 84–104.
6. Williamson, R.V. The Flow of Pseudoplastic Materials. *Ind. Eng. Chem.* **1929**, *21*, 1108–1111. [CrossRef]
7. Sakiadis, B.C. Boundary-layer behavior on continuous solid surfaces: I. Boundary-layer equations for two-dimensional and axisymmetric flow. *AIChE J.* **1961**, *7*, 26–28. [CrossRef]
8. Crane, L.J. Flow past a stretching plate. *Z. Angew. Math. Phys. ZAMP* **1970**, *21*, 645–647. [CrossRef]
9. Khan, S.; Selim, M.M.; Khan, A.; Ullah, A.; Abdeljawad, T.; Ikramullah; Ayaz, M.; Mashwani, W.K. On the Analysis of the Non-Newtonian Fluid Flow Past a Stretching/Shrinking Permeable Surface with Heat and Mass Transfer. *Coatings* **2021**, *11*, 566. [CrossRef]
10. Zeb, H.; Bhatti, S.; Khan, U.; Wahab, H.A.; Mohamed, A.; Khan, I. Impact of Homogeneous-Heterogeneous Reactions on Flow of Non-Newtonian Ferrofluid over a Stretching Sheet. *J. Nanomater.* **2022**, *2022*, 2501263. [CrossRef]
11. Mahabaleshwar, U.S.; Maranna, T.; Sofos, F. Analytical investigation of an incompressible viscous laminar Casson fluid flow past a stretching/shrinking sheet. *Sci. Rep.* **2022**, *12*, 18404. [CrossRef]
12. Abbas, N.; Nadeem, S.; Shatanawi, W. Effects of radiation and heat generation for non-Newtonian fluid flow over slendering stretching sheet: Numerically. *J. Appl. Math. Mech.* **2022**, *103*, e202100299. [CrossRef]
13. Akbar, N.S.; Al-Zubaidi, A.; Saleem, S.; Alsallami, S.A.M. Variable fluid properties analysis for thermally laminated 3-dimensional magnetohydrodynamic non-Newtonian nanofluid over a stretching sheet. *Sci. Rep.* **2023**, *13*, 3231. [CrossRef]
14. Masuda, H.; Ebata, A.; Teramae, K.; Hishinuma, N. Alteration of Thermal Conductivity and Viscosity of Liquid by Dispersing Ultra-Fine Particles. Dispersion of Al2O3, SiO2 and TiO2 Ultra-Fine Particles. *Netsu Bussei* **1993**, *7*, 227–233. [CrossRef]
15. Choi, S.U.S.; Eastman, J.A. Enhancing thermal conductivity of fluids with nanoparticle. In Proceedings of the 1995 International Mechanical Engineering Congress and Exhibition, San Francisco, CA, USA, 12–17 November 1995.
16. Elboughdiri, N.; Ghernaout, D.; Muhammad, T.; Alshehri, A.; Sadat, R.; Ali, M.R.; Wakif, A. Towards a novel EMHD dissipative stagnation point flow model for radiating copper-based ethylene glycol nanofluids: An unsteady two-dimensional homogeneous second-grade flow case study. *Case Stud. Therm. Eng.* **2023**, *45*, 102914. [CrossRef]
17. Ashraf, M.Z.; Rehman, S.U.; Farid, S.; Hussein, A.K.; Ali, B.; Shah, N.A.; Weera, W. Insight into Significance of Bioconvection on MHD Tangent Hyperbolic Nanofluid Flow of Irregular Thickness across a Slender Elastic Surface. *Mathematics* **2022**, *10*, 2592. [CrossRef]
18. Nabwey, H.A.; Rahbar, F.; Armaghani, T.; Rashad, A.M.; Chamkha, A.J. A Comprehensive Review of Non-Newtonian Nanofluid Heat Transfer. *Symmetry* **2023**, *15*, 362. [CrossRef]
19. Selimefendigil, F.; Şenol, G.; Öztop, H.F.; Abu-Hamdeh, N.H. A Review on Non-Newtonian Nanofluid Applications for Convection in Cavities under Magnetic Field. *Symmetry* **2022**, *15*, 41. [CrossRef]
20. Lou, Q.; Ali, B.; Rehman, S.U.; Habib, D.; Abdal, S.; Shah, N.A.; Chung, J.D. Micropolar Dusty Fluid: Coriolis Force Effects on Dynamics of MHD Rotating Fluid When Lorentz Force Is Significant. *Mathematics* **2022**, *10*, 2630. [CrossRef]

21. Alfven, H. Existence of Electromagnetic-Hydrodynamic Waves. *Nature* **1942**, *150*, 405–406. [CrossRef]

22. Abbas, A.; Jeelani, M.B.; Alnahdi, A.S.; Ilyas, A. MHD Williamson Nanofluid Fluid Flow and Heat Transfer Past a Non-Linear Stretching Sheet Implanted in a Porous Medium: Effects of Heat Generation and Viscous Dissipation. *Processes* **2022**, *10*, 1221. [CrossRef]

23. Reddy C, S.; Naikoti, K.; Rashidi, M.M. MHD flow and heat transfer characteristics of Williamson nanofluid over a stretching sheet with variable thickness and variable thermal conductivity. *Trans. A. Razmadze Math. Inst.* **2017**, *171*, 195–211. [CrossRef]

24. Shawky, H.M.; Eldabe, N.T.M.; Kamel, K.A.; Abd-Aziz, E.A. MHD flow with heat and mass transfer of Williamson nanofluid over stretching sheet through porous medium. *Microsyst. Technol.* **2019**, *25*, 1155–1169. [CrossRef]

25. Bouslimi, J.; Omri, M.; Mohamed, R.A.; Mahmoud, K.H.; Abo-Dahab, S.M.; Soliman, M.S. MHD Williamson nanofluid flow over a stretching sheet through a porous medium under effects of joule heating, nonlinear thermal radiation, heat generation/absorption, and chemical reaction. *Adv. Math. Phys.* **2021**, *2021*, 9950993. [CrossRef]

26. Hayat, T.; Bashir, G.; Waqas, M.; Alsaedi, A. MHD 2D flow of Williamson nanofluid over a nonlinear variable thicked surface with melting heat transfer. *J. Mol. Liq.* **2016**, *223*, 836–844. [CrossRef]

27. Ibrahim, W.; Negera, M. The Investigation of MHD Williamson Nanofluid over Stretching Cylinder with the Effect of Activation Energy. *Adv. Math. Phys.* **2020**, *2020*, 9523630. [CrossRef]

28. Eswara Rao, M.; Siva Sankari, M.; Nagalakshmi, C.; Rajkumar, S. On the Role of Bioconvection and Activation Energy for MHD-Stretched Flow of Williamson and Casson Nanofluid Transportation across a Porous Medium Past a Permeable Sheet. *J. Nanomater.* **2023**, *2023*, 3995808. [CrossRef]

29. Asjad, M.I.; Zahid, M.; Ali, B.; Jarad, F. Unsteady MHD Williamson Fluid Flow with the Effect of Bioconvection over Permeable Stretching Sheet. *Math. Probl. Eng.* **2022**, *2022*, 7980267. [CrossRef]

30. Wang, F.; Asjad, M.I.; Rehman, S.U.; Ali, B.; Hussain, S.; Gia, T.N.; Muhammad, T. MHD Williamson Nanofluid Flow over a Slender Elastic Sheet of Irregular Thickness in the Presence of Bioconvection. *Nanomaterials* **2021**, *11*, 2297. [CrossRef]

31. Ahmed, K.; Akbar, T.; Muhammad, T.; Alghamdi, M. Heat transfer characteristics of MHD flow of Williamson nanofluid over an exponential permeable stretching curved surface with variable thermal conductivity. *Case Stud. Therm. Eng.* **2021**, *28*, 101544. [CrossRef]

32. Patil, V.S.; Humane, P.P.; Patil, A.B. MHD Williamson nanofluid flow past a permeable stretching sheet with thermal radiation and chemical reaction. *Int. J. Model. Simul.* **2023**, *43*, 185–199. [CrossRef]

33. Khan, M.; Malik, M.Y.; Salahuddin, T.; Hussian, A. Heat and mass transfer of Williamson nanofluid flow yield by an inclined Lorentz force over a nonlinear stretching sheet. *Results Phys.* **2018**, *8*, 862–868. [CrossRef]

34. Kumar, P.B.S.; Gireesha, B.J.; Gorla, R.S.R.; Mahanthesh, B. Magnetohydrodynamic Flow of Williamson Nanofluid Due to an Exponentially Stretching Surface in the Presence of Thermal Radiation and Chemical Reaction. *J. Nanofluids* **2017**, *6*, 264–272. [CrossRef]

35. Nadeem, S.; Hussain, S.T.; Lee, C. Flow of a Williamson fluid over a stretching sheet. *Braz. J. Chem. Eng.* **2013**, *30*, 619–625. [CrossRef]

36. Ahmed, K.; Akbar, T. Numerical investigation of magnetohydrodynamics Williamson nanofluid flow over an exponentially stretching surface. *Adv. Mech. Eng.* **2021**, *13*, 168781402110198. [CrossRef]

37. Amjad, M.; Ahmed, I.; Ahmed, K.; Alqarni, M.S.; Akbar, T.; Muhammad, T. Numerical Solution of Magnetized Williamson Nanofluid Flow over an Exponentially Stretching Permeable Surface with Temperature Dependent Viscosity and Thermal Conductivity. *Nanomaterials* **2022**, *12*, 3661. [CrossRef]

38. Li, Y.-X.; Alshbool, M.H.; Lv, Y.-P.; Khan, I.; Riaz Khan, M.; Issakhov, A. Heat and mass transfer in MHD Williamson nanofluid flow over an exponentially porous stretching surface. *Case Stud. Therm. Eng.* **2021**, *26*, 100975. [CrossRef]

39. Motsa, S.S.; Dlamini, P.G.; Khumalo, M. Spectral Relaxation Method and Spectral Quasilinearization Method for Solving Unsteady Boundary Layer Flow Problems. *Adv. Math. Phys.* **2014**, *2014*, 341964. [CrossRef]

40. Nadeem, S.; Hussain, S.T. Heat transfer analysis of Williamson fluid over exponentially stretching surface. *Appl. Math. Mech.* **2014**, *35*, 489–502. [CrossRef]

41. Dapra, I.; Scarpi, G. Perturbation solution for pulsatile flow of a non-Newtonian Williamson fluid in a rock fracture. *Int. J. Rock Mech. Min. Sci.* **2007**, *44*, 271–278. [CrossRef]

42. Rosseland, S. *Theoretical Astrophysics*; Oxford University Press: Oxford, UK, 1936.

43. Seini, Y.I.; Makinde, O.D. MHD Boundary Layer Flow due to Exponential Stretching Surface with Radiation and Chemical Reaction. *Math. Probl. Eng.* **2013**, *2013*, 163614. [CrossRef]

44. Bellman, R.; Kalaba, R. *Quasilinearization and Nonlinear Boundary-Value Problems*; American Elsevier Publishing Company: New York, NY, USA, 1965.

45. Amjad, M.; Ahmed, K.; Akbar, T.; Muhammad, T.; Ahmed, I.; Alshomrani, A.S. Numerical investigation of double diffusion heat flux model in Williamson nanofluid over an exponentially stretching surface with variable thermal conductivity. *Case Stud. Therm. Eng.* **2022**, *36*, 102231. [CrossRef]

46. Motsa, S. On the New Bivariate Local Linearisation Method for Solving Coupled Partial Differential Equations in Some Applications of Unsteady Fluid Flows with Heat and Mass Transfer. In *Mass Transfer—Advancement in Process Modelling*; InTech: Vienna, Austria, 2015. [CrossRef]

47. Alharbey, R.A.; Mondal, H.; Behl, R. Spectral Quasi-Linearization Method for Non-Darcy Porous Medium with Convective Boundary Condition. *Entropy* **2019**, *21*, 838. [CrossRef]